Mapping of coal properties and gas content in east Bokaro coalbed methane reservoir

Abir Banerjee, Ramchandra Soren, Shyam Hembrom, Gautam Bhattacharya, Nawin Lugun, Aloke Das
Oil and Natural Gas Corporation Ltd.
Corresponding author email: *Banerjee_Abir@ongc.co.in*

Keywords

Proximate analysis; Gas content; Regression equation; Low resistivity formation; Contour map

Abstract

The eastern part of the Bokaro coalbed methane reservoir shows heterogeneity and complexity in geological formation during drilling wells. The geological surprises include the observation of very low resistivity formation, missing coal seam, thickness variation of coal, carbon dioxide (CO_2) generation during production, and comparative variation of gas content in the seam. Several maps were generated based on the well log analysis from 91 wells in the study area. The path of a very low resistive signature shows an NW-SE trend which is observed below the Kargali Top seam and this affects the coal quality. Interestingly, the fault lines could easily be identified from the number of five objective coal seam and cumulative thickness contour map. During the production stage, it was observed that CO_2 gas is also produced along with methane gas, and therefore data was compiled to map CO_2 percentage. A methodology was applied to determine the seam-wise gas content based on the obtained regression equation from density and gamma ray log data with proximate analysis of the core sample, available in a few wells. Gas content using Kim's equation was determined and relations between fixed carbon/volatile matter versus gas content were obtained in coal. A good correlation exists between the gas content estimated from Kim's model and observed gas content from desorption studies. Subsequently, the equations were propagated to other wells to generate individual seam map. The result from the study illustrates a holistic view of the coal seam in terms of quality that helps to place potential future well locations to maximize gas production. The proximate and gas content can be estimated based on developed methodology, where core studies are unavailable. Also, it gives scope to investigate the feasibility of CO_2 capture and sequestration and enhanced coal seam gas recovery using CO_2 injection methodology.

Introduction

In unconventional reservoirs such as coalbed methane (CBM), the production stages from coal seams differ from conventional reservoirs. The coal seam acts as the source, reservoir, and cap rock of the gas reserve in the adsorbed state. During production from the coal seam, initial dewatering continues; followed by the gas break. In achieving a gas break, wells require continuous dewatering until the pressure reaches the desorption pressure, which is the critical limit in achieving the gas break. Once the gas break is achieved, the gas production increases and the water production declines over the life cycle of the well. Coal seam gas primarily contains methane gas (90%) and the rest (10%) constitutes of ethane, propane, carbon dioxide, nitrogen, and a few other gases. A higher concentration of CO_2 is not viable for gas sales and it also leads to corrosion of pipes and storage tanks. Although, the gas content in coal is dependent on several factors such as pressure, temperature, the rank of coal, depth of burial, and maceral and proximate content. Coal is composed of both organic and inorganic content; organic content constitutes of fixed carbon (FC) and volatile matter (VM) while the inorganic part is composed of ash (A) and moisture content (MC). Gas content in coal seams is a significant factor in determining the gas reserve and feasibility of the reservoir development (Banerjee and Chatterjee, 2021). The desorption study of the core sample in the laboratory is the most accurate method for estimating the gas content in the coal. However, as there are constraints in the extraction of core samples from every well, hence core sample test is limited to a few key wells. Therefore, to draw a larger picture of gas content estimation, previously numerous empirical equations from the proximate analysis have been developed specifically for areas and seams. Kim's (1977) and Meisner's (1984) equations are widely accepted and

used in the estimation of gas content. The study area lies in the east Bokaro coalfield, located in the state of Jharkhand in the eastern part of India; contains 91 wells in 20 Km^2. Banerjee and Chatterjee, 2021 have discussed the details of the geological formations, stratigraphy, and extension of the east Bokaro coalfield and the formations exhibit heterogeneity and geological surprises in the depth variation of Barakar coal seams, missing coal seams at several locations, fault pattern ranging from micro-to-macro, presence of very low resistivity formation (0.2-0.5 Ohmm) below coal seam, and lateral variation of gas content form seams in the production phase of different wells. Moreover, the investigation of the problems faced becomes challenging due to the limitations of broader data sources. The datasets consist of (i) conventional well logs (gamma ray, resistivity, density, and neutron porosity), (ii) proximate analysis (A, M, FC, and VM), (iii) gas content (GC) from desorption studies, and (iv) production testing result. Given the above, the objective of the study includes (a) structure mapping of very low resistivity formation, (b) observed coal seam and cumulative seam thickness mapping, (c) carbon dioxide generated map from wells, and (d) developing regressing equation between proximate and gas content using core studies and well log parameters, (e) seam-wise mapping of lateral variation of proximate and gas content.

Methods

Proximate analysis is a method to determine the percentage content of organic and inorganic content, which includes A, M, FC and VM (Zhu, 2014). Also, gas content (GC) was estimated from the desorption studies (Diamond and Levine, 1981; Moore and Butland, 2005). Both, the proximate and gas content data were derived from laboratory testing and these were available in only seven wells and the rest of the wells does not contain. The steps in the desorption procedure include: (a) quickly bringing coal samples onto the surface, (b) sealing samples in a leak-proof canister, and (c) measuring desorbed and residual gas using manometer and pulverizer equipment Therefore, a methodology was adopted to establish a few relationships; i.e. A, M, FC, VM, and GC versus well log parameters. The GC was also estimated by Kim (1977) and Meisner (1984) to understand the variation of actual and predicted gas content.

Estimation of in-situ gas content of the coal evaluated using Kim's equation as follows:

$$GC_K = 0.75 * \left[\frac{FC+VM}{100}\right] * (X - Y), \quad (1)$$

Where the parameter X and Y are expressed as:

$$X = [0.8 * (FC/VM) + 5.6] * (0.095 * depth)^{N_0}, \quad (2)$$

$$Y = 0.14 * (0.18 * depth/100 + 11), \quad (3)$$

Where, N_0 is represented as:

$$N_0 = [0.315 - 0.01 * (FC/VM)], \quad (4)$$

The Meinser equation is related to the VM (daf) which estimates the volume of the gas content as:

$$GC_M = -325.6 * \log(VM/37.8), \quad (5)$$

From equations (4) and (5), the GC estimated are compared, and the following methodology was followed; if $GC_K < GC_M$, then $GC = GC_K$, and if $GC_K > GC_M$, then $GC = GC_M$. In core samples, measured gas content were available from laboratory test, hence to validate the Kim's gas content estimated from the equation (1), figure 1 was plotted to verify the accuracy of the estimation from the cross-plot between measured and estimated gas content.

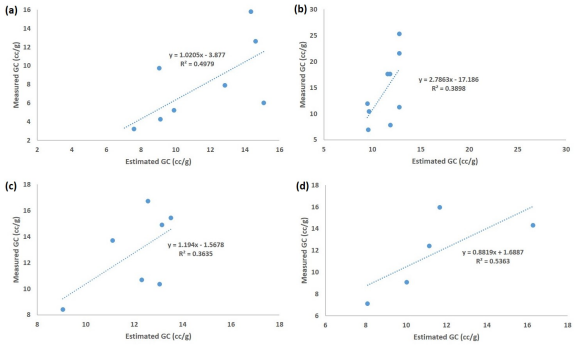

Figure 1. Crossplot between estimated and measured gas content in (a) Karo-VIII seam, (b) Bermo seam, (c) Kargali Bottom, and (d) Kargali Top.

Density and gamma ray log was used in establishing the relationship. In our study, four objective coal seams were considered and for each seam, equations were developed. These regression equations were propagated to other wells in generation maps. The first relation was established between (i) A and the density log, and the second relation was established between (ii) FC and A. In the third relation, (iii) gamma ray was plotted with (FC+VM). Hence from this plot VM is determined by subtracting

[(FC+VM)- FC]. The sum of organic and inorganic content in coal constitutes 100%, therefore the M content was determined by subtracting the sum of the three proximate content with cent percent. Table 1 tabulates the seam-wise equations which were established from the cross-plot. One such example is shown in figure 2 which illustrates the four plots for the Bermo coal seam, and each plot establishes a regression equation between two parameters and fitting coefficient (R^2).

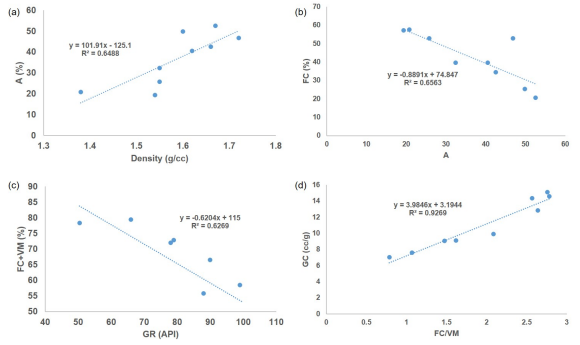

Figure 2. Crossplot between proximate and well log parameters and the best-fit equation and regression coefficient. (a) A vs. density, (b) FC vs. Ash, (c) (FC+VM) vs. GR, and (d) GC vs. FC/VM.

Table 1. Seam-wise description of plots tabulating coal seam, establishes equations and the fitting coefficient (R_2) of each equation.

Seam	Equation	R^2
Kargali Top	A = 15.165*D + 0.7121	0.77
	FC = 2.9089*A - 16.103	0.69
	(FC+VM) = -0.0263*GR + 81.352	0.47
	GC = 4.1209*(FC/VM) + 3.9799	0.87
Kargali Bottom	A = 16.12*D + 2.034	0.58
	FC = -0.6211*A + 72.754	0.46
	(FC+VM) = -0.011*GR + 83.111	0.04
	GC = 1.9502*(FC/VM) + 8.0276	0.63
Bermo	A = 32.149*D - 23.43	0.70
	FC = -0.6279*A + 64.451	0.64
	(FC+VM) = -0.0063*GR^2 + 0.9963*GR + 36.265	0.70
	GC = 89.987*(FC/VM)^3 - 561.19*(FC/VM)^2 + 1151*(FC/VM) - 763.35	0.84
Karo-VIII	A = 101.91*D - 125.1	0.65
	FC = -0.8891*A+ 74.847	0.66
	(FC+VM) = -0.6204*GR + 115	0.63
	GC = 3.9846*(FC/VM) + 3.1944	0.93

Formations and coal seams were correlated in true vertical depth using well logs of 91 wells. One such marker is the very low resistivity zone, which is observed in a few wells below the Kargali top seam. Accordingly, the depth was accounted for the structural modeling using the top depth. Based on well log correlation, cumulative seam thickness was determined for each well. The correlation of very low resistivity formation in vicinity of Kargali top seam for 13 wells is shown in figure 3. The low resistivity zone are prone to fractures as conducting mineral deposition have deposited at the time of volcanic eruption. The thickness of this zone varies from 1 m to 10 m respectively and it is observed that the gas content in the Kargali Top is low and there is a higher dewatering rate. Figure 4 represents correlated profile of 13 wells in the location map of the east Bokaro coalfield as shown in the well correlation map. The contours map were generated by integrating data from 91 wells based on an advanced grid interpolation algorithm. The detailed parameters from the well include: latitude, longitude, depth, and thickness of the low resistivity zone, the number of objective coal seams observed in wells, the cumulative thickness of coal seams in wells, and the percentage of carbon dioxide produced from wells. Additionally, proximate and gas content parameters were integrated in the seam-wise mapping to understand the lateral variation in coal seam. The proximate and gas content were estimated from the established equations based on deterministic approach as tabulated in table 1.

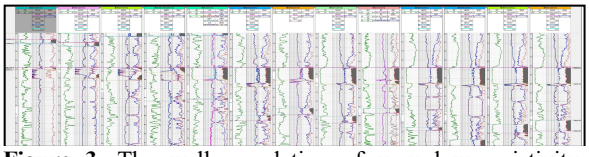

Figure 3. The well correlation of very low resistivity formation below the Kargali Top coal seam of 13 wells, where the resistivity lies from 0.2-0.5 Ohm-m.

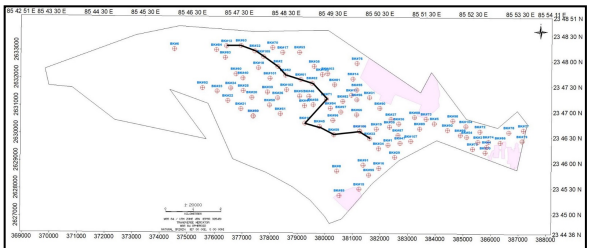

Figure 4. The location map of the east Bokaro coalfield with wells position and the black lines connecting the 13 wells were correlated as shown in the well correlation map.

Results and Discussions

The data incorporated from the well log correlation and production data were used to generate four separate contour maps. Figure 5 shows contour maps of (a) very low resistivity formation, (b) the number of the observed coal seam, (c) the cumulative thickness of the objective coal seam, and (d) CO_2 production distribution. In Figure 5a, a contour map illustrating very low resistivity formation is presented in sub-surface true vertical depth, where the formation varies from 100m to 900 m. The structural representation of very low resistive formation depicts, the formation in the NW region is at shallower depth and is gradually moving towards a deeper along the SE direction. Hence, the structural trend of this formation lies in the NW-SE direction i.e. the direction of the minimum horizontal stress direction, as corroborated with the local tectonic stress from the resistivity image log. These areas contained weak planes or fractured where the mineral deposition took place. The low resistivity signature is prone to high water production Kargali Top coal seam as observed during the production stage. This can occur due to the channeling and connectivity to the aquifer zone. The X-ray diffraction studies of the side wall core sample extracted from this formation quantify the presence of conducting minerals such as siderite and pyrite. This secondary mineral deposition adds to the very low resistivity formation and this has occurred during the volcanic eruption. The trend from the map shows that the origin of the volcanic matter is on the NW side at shallower depth and the lava flows gradually towards the SE side at the shallower part. Also, it can be concluded that the flow and deposition of minerals have occurred along the fractured or weak formation; hence the trend signifies the NW-SE fracture along the minimum horizontal stress. The general maximum horizontal stress is along the NE-SW direction as confirmed by the world stress map and drilling-induced fractures in the resistivity image log. In Figure 5b, the contour map represents the number of objective coal seams observed from well log correlation. This map signifies the variation of the missing coal seam in the area that indicates the possible fault pattern and direction. A major NW-SE fault and several small fault pattern in the NE-SW direction is predictable. The missing coal seams in the entire patch of east Bokaro coalfield can be due to pinch-out of the coal seam or the well trajectory passing through the possible fault plane. The trend of the observed all objective coal seams and missing coal seams develop the possible fault line in the area. Another inference from the figure is the complete absence of objective seam in the central NW-SE trend where geological surprises occur. There can be two possibilities; either the structure is graben with a high throw or complete absence of fluvial deposition. In Figure 5c, the distribution of cumulative coal seam thickness is presented in the map. Considering figure 5b and 5c, these map gives an overall view of the prospective location for future drilling where we can hit the maximum number of objective coal seams with greater thickness. In Figure 5d, the CO_2 distribution from wells is shown. The production from wells yields different CO_2 concentrations, and the higher yield of CO_2 is a cause for concern in terms of the greenhouse effect on the environment, gas sales, calorific value of gas, and corrosive properties of CO_2 in pipelines and containers. The higher percentage of CO_2 is prone to the rusting of pipelines and does not meet the standard criteria for gas sales. Therefore, the map view helps to plan and separate CO_2 gas accordingly.

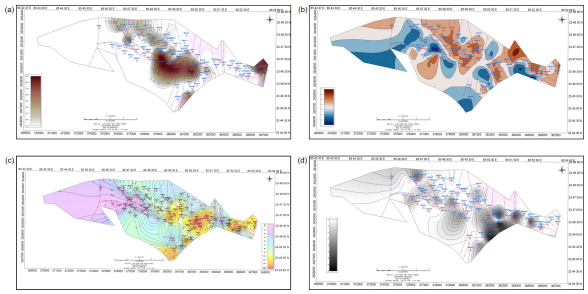

Figure 5. Contour map of the patch representing the variation of (a) the depth trend of the low resistivity

formation, (b) the observed number of objective coal seams, (c) variation of cumulative coal seam thickness, and (d) carbon dioxide distribution in the area.

The proximate analysis map was generated based on the empirical equation developed from the regression equation. Four seams were studied in ascending depth order; (i) Kargali Top, (ii) Kargali Bottom, (iii) Bermo, and (iv) Karo-VIII. Each seam-wise map is prepared to study the variation in A, M, FC, VM, and GC. The Ash content contour map of each seam is presented in figure 6 (a-d). The deposition of Ash content in Kargali Top is lower compared to Kargali Bottom and Bermo, while it is lowest in Karo-VIII. Similarly, the M, FC, and VM content for all four seams are represented in figure 7 (a-d), figure 8 (a-d), and figure 9 (a-d) respectively. The M content varies from 1-4% respectively in all the four seams, the higher side of the M is shown in deep brown color and the lower range in lighter brown colour. Altogether, the northern part in Karo-VIII have lower M, the central and southern part in Bermo have lower M, the eastern part in Kargali Bottom have lower M and the southern eastern part have low M. FC content is higher with few low lobes in Karo-VIII, Bermo has lower FC considerably, the central and south eastern part have low FC, and constant medium FC is observed in Kargali Top. Both high and low VM content is observed in Karo-VIII, the VM is higher throughout but highest lobes are also observed in Bermo, the northern and southern part contain low VM in Kargali Bottom, and considerably low GC is observed Kargali Top seam. In general, it has been observed that the NE-SW and or NW-SE of proximate trend is observed. This can be depositional flow direction existing at the formation of coal. Subsequently, the most significant parameter that is the GC in each seam obtained from the relationship between Kim's method and the ratio of organic content (FC/VM) is plotted in the contour map (figure 10 (a-d)). The GC in higher in few patches in western, south central and eastern part in Karo-VIII, GC is higher in the east-central part in Bermo, the peripheral part in the Kargali Bottom have higher GC and the GC remains constantly high Kargali Top seam. Table 2 tabulates the seam-wise range and variation of proximate parameters in % such as A, M, FC, and VM. Also, the respective range of GC is presented which varies from 5-24 cc/g.

Table 2. The table tabulates the range of proximate parameters (A, M, FC, VM) in % and GC in cc/g for seam-wise (Kargali Top, Kargali Bottom, Bermo and Karo-VIII).

Seam	A (%)	M (%)	FC (%)	VM (%)	GC (cc/g)
Kargali Top	10-20	10-20	10-20	10-20	10-20
Kargali Bottom	10-20	10-20	10-20	10-20	10-20
Bermo	17-27	0.1-3.8	44-53	18-29	10-23
Karo-VIII	21-48	0.1-3.7	32-54	16-34	5-24

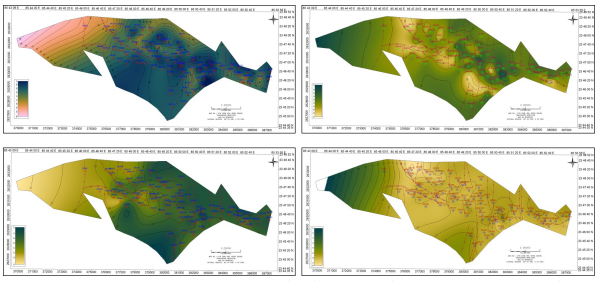

Figure 6. Contour map of the patch representing the variation of ash content in (%) for seams: (a) Karo-VIII, (b) Bermo, (c) Kargali Bottom, and (d) Kargali Top.

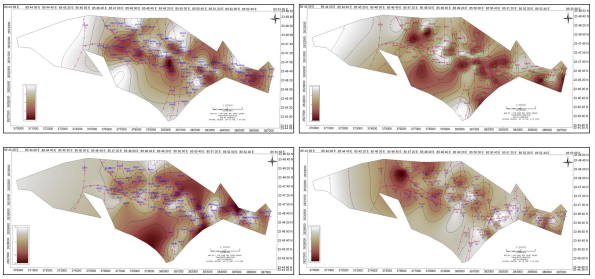

Figure 7. Contour map of the patch representing the variation of moisture content in (%) for seams: (a) Karo-VIII, (b) Bermo, (c) Kargali Bottom, and (d) Kargali Top.

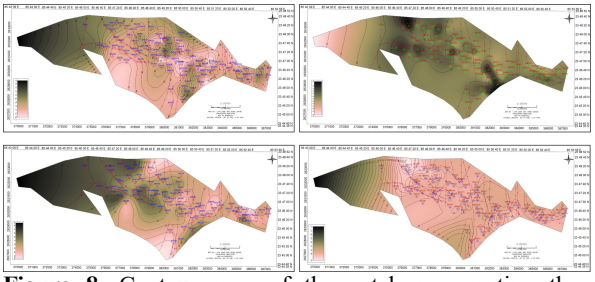

Figure 8. Contour map of the patch representing the variation of fixed carbon content in (%) for seams: (a)

Karo-VIII, (b) Bermo, (c) Kargali Bottom, and (d) Kargali Top.

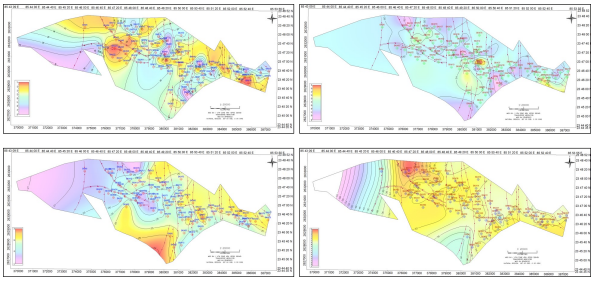

Figure 9. Contour map of the patch representing the variation of volatile matter in (%) for seams: (a) Karo-VIII, (b) Bermo, (c) Kargali Bottom, and (d) Kargali Top.

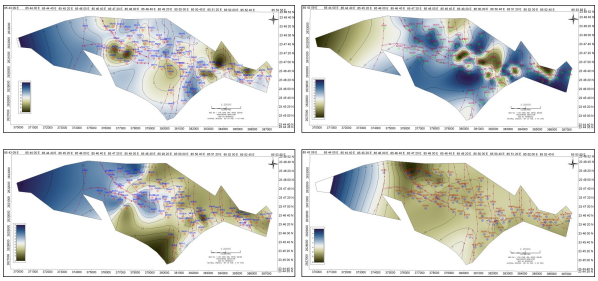

Figure 10. Contour map of the patch representing the variation of gas content in (cc/g) for seams: (a) Karo-VIII, (b) Bermo, (c) Kargali Bottom, and (d) Kargali Top.

Conclusions

The missing gap in the structural and geological knowledge in the sub-surface has been enhanced from the present study. These are as follows:

(i) The very low resistivity formation provides the idea about the lava flow, depth, and continuation in the area. Hence, a pre-geological model can be designed before drilling.

(ii) Infill wells can be placed from the study based on the integrated approach from the number of the objective seam and cumulative thickness map.

(iii) The contour map of proximate parameters presents the lateral variation of the organic and inorganic content in each coal seam. This gives an idea about the coal quality and maturation. Also, the gas content map helps to point out the areas where the higher gas content exists. The gas content linearly increases with an increase in the ratio of FC/VM.

(iv) This study also presents a methodology to estimate the proximate and gas content in coal seams from the developed equations where core data is unavailable.

(v) The identification of the areas with a higher percentage of carbon dioxide production will help to plan and modify the strategy to separate the carbon dioxide from methane gas. Also, research and development work on CO2 methane-enhanced recovery and sequestration in coal seams are the future focus.

References

Banerjee, A., and Chatterjee, R., 2021, Fracture analysis using Stoneley wave in a coalbed methane reservoir; Near Surface Geophysics.

Diamond, W.P., and Levine, J.R., 1981, Direct method determination of the gas content of coal: Procedures and results (p.36). U.S: Bureau of Mines, Washington, D.C.

Kim, A. G., 1977, Estimating methane content of bituminous coalbeds from adsorption data; Report of investigation 8245, U.S. Bureau of Mines, Washington DC (pp. 22).

Moore, T.A., and Butland, C.I., 2005, Coal seam gas in New Zealand as a model for Indonesia. In: S. Prihatmoko, S. Digdowirogo, C. Nas, T. V. Leeuwen, & H. Widjajanto (Eds.), Indonesian Mineral and Coal Discoveries (pp. 192–200). Bogor: Indonesian Association of Geologists.

Zhu, Q., 2014, Coal sampling and analysis standards; London: IEA Clean Coal Centre.

Acknowledgment

Authors are grateful to ONGC Ltd. for the permission to conduct the study and present the technical paper.